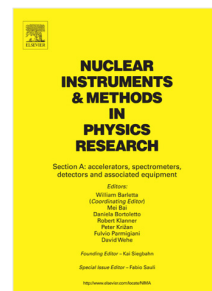


Accepted Manuscript

From optical to X-ray ghost imaging

Thomas A. Smith, Yanhua Shih, Zhehui Wang, Xuan Li,
Bernhard Adams, Marcel Demarteau, Robert Wagner, Junqi Xie,
Lei Xia, Ren-Yuan Zhu, Liyuan Zhang, Chen Hu



PII: S0168-9002(19)30643-6
DOI: <https://doi.org/10.1016/j.nima.2019.05.027>
Reference: NIMA 62186

To appear in: *Nuclear Inst. and Methods in Physics Research, A*

Received date: 8 December 2018
Revised date: 24 April 2019
Accepted date: 8 May 2019

Please cite this article as: T.A. Smith, Y. Shih, Z. Wang et al., From optical to X-ray ghost imaging, *Nuclear Inst. and Methods in Physics Research, A* (2019), <https://doi.org/10.1016/j.nima.2019.05.027>

This is a PDF file of an unedited manuscript that has been accepted for publication. As a service to our customers we are providing this early version of the manuscript. The manuscript will undergo copyediting, typesetting, and review of the resulting proof before it is published in its final form. Please note that during the production process errors may be discovered which could affect the content, and all legal disclaimers that apply to the journal pertain.

- Point-to-point ghost imaging is a result of two-photon interference
- X-ray ghost imaging provides higher resolution images than traditional imaging
- A correct setup may allow for turbulence-free X-ray ghost imaging

From Optical to X-ray Ghost Imaging

Thomas A. Smith*, and Yanhua Shih

*Department of Physics, University of Maryland, Baltimore County, Baltimore, MD 21250,
USA*

Zhehui Wang and Xuan Li

Los Alamos National Laboratory, Los Alamos, NM 87545, USA

Bernhard Adams

Incom, Inc., Charlton, MA 01507, USA

Marcel Demarteau, Robert Wagner, Junqi Xie, and Lei Xia

Argonne National Laboratory, Lemont, IL 60439, USA

Ren-Yuan Zhu, Liyuan Zhang, and Chen Hu

256-48, HEP, California Institute of Technology, Pasadena, CA 91125, USA

Abstract

Recent advances in ghost imaging techniques and X-ray sources such as synchrotrons and, more recently X-ray free-electron lasers (XFEL) have made X-ray ghost imaging a growing topic of interest. One specific type of ghost imaging utilizes thermal radiation and the measurement of intensity fluctuation correlation to form a true image without the need of a lens. This technique allows for much higher resolution than traditional X-ray imaging for a mesoscopic or even a microscopic object. In addition to this benefit of not requiring a lens, a surprising experiment has shown that, when set up correctly, this type of ghost imaging can provide clear images through the measurement of intensity fluctuation correlation when traditional images through measurements of intensity are blurred due to optical turbulence and vibrations. This turbulence-free technique will help maintain the high resolution of X-ray ghost imaging. How is an image formed from fluctuations in light? And what makes it turbulence-free? Using the concept of two-photon interference, this article provides an introduction to

*tsmith25@umbc.edu
Preprint submitted to Elsevier

these fundamentally interesting concepts and X-ray ghost imaging.

14 *Keywords:*

15 Optics, Imaging, Quantum Optics, Ghost Imaging, X-rays, Synchrotron

16 1. Introduction

17 The first demonstration of ghost imaging was accomplished by Pittman *et*
18 *al.* with the measurement of coincidence counts of entangled photon pairs in-
19 cident on two separate detectors [1]. Shortly following, efforts were made to
20 develop ghost imaging with thermal light [2]. Due to how common thermal
21 light is (generated by the sun, light bulbs, and many other sources), ghost
22 imaging with thermal light is more accessible than ghost imaging with entan-
23 gled light. Valencia *et al.* were able to achieve ghost imaging with thermal light
24 through the measurement of intensity fluctuation correlation. Unlike mean in-
25 tensity measurements, which is a result of single-photon interference, intensity
26 fluctuation correlation is a measurement of two-photon interference, or a pair
27 of photons interfering with the pair itself [3]. This type of ghost imaging also
28 does not require the use of a lens, as the image is formed directly from the
29 correlation. Taking advantage of this feature, we can extend ghost imaging to
30 X-ray regime which have much higher penetrating power than optical photons
31 and are unaffected by additional lenses. Applying X rays will allow for higher
32 resolution images with the potential for angstrom-level resolution.

33 To model ghost imaging and two-photon interference, we will utilize Ein-
34 stein's theory of light. Einstein introduced granularity to light by theorizing
35 that, instead of long, continuous electromagnetic waves, it consisted of many
36 individual subfields (now known as photons) emitted by many subsources (now
37 known as atomic transitions) [4]. For thermal light (which is used throughout
38 this paper), these subfields are emitted randomly with a random phase. While
39 the quantum picture would adequately explain these phenomena, it has been
40 known that the effective wave function of a photon in the thermal state is math-
41 ematically the same function as Einstein's subfield model, so we will focus on

42 the latter [5–8]. When many subfields, represented by E_m , are present at one
 43 location, the total electric field is the superposition of each subfield,

$$E(\mathbf{r}, t) = \sum_m E_m(\mathbf{r}, t) = \sum_m \int d\omega E_m(\omega) g_m(\omega; \mathbf{r}, t), \quad (1)$$

44 for which

$$E_m(\omega) = a_m(\omega) e^{i\psi_m(\omega)}, \quad (2)$$

45 where $a_m(\omega)$ is the amplitude and $\psi_m(\omega)$ is the random initial phase of the
 46 subfield. The Green's function, $g_m(\omega; \mathbf{r}, t)$, is used as a “propagator” which
 47 represents propagations from the m 'th subsource located at (\mathbf{r}_m, t_m) to a sepa-
 48 rate point in spacetime at (\mathbf{r}, t) . The Green's function varies depending on the
 49 path of propagation. Here we will approximate ghost imaging as a near field
 50 measurement and also only focus on the spatial portion of the Green's function.
 51 Written in terms of the transverse coordinate $\boldsymbol{\rho}$, the near-field spatial Green's
 52 function is

$$g_m(\omega; \boldsymbol{\rho}, z) = \frac{-i\omega}{2\pi c} \frac{e^{i\frac{\omega}{c}z}}{z} e^{i\frac{\omega}{2cz}|\boldsymbol{\rho}-\boldsymbol{\rho}_m|^2}. \quad (3)$$

53 The measurement of intensity at a single detector located at (\mathbf{r}, t) , is represented
 54 by the expectation value or ensemble average of intensity, $\langle I(\mathbf{r}, t) \rangle$. Intensity
 55 is an amplitude-amplitude correlation which, using Glauber's formalism, is also
 56 known as first order correlation, $\Gamma^{(1)}(\mathbf{r}, t)$. This measurement is the total electric
 57 field correlated with itself, thus correlating all of the subfields with themselves
 58 ($m = n$) and all others ($m \neq n$). It is convenient to split our intensity term
 59 into these two separate cases,

$$\begin{aligned}
\Gamma^{(1)}(\mathbf{r}, t) &= \langle I(\mathbf{r}, t) \rangle = \langle E^*(\mathbf{r}, t)E(\mathbf{r}, t) \rangle \\
&= \left\langle \sum_m E_m^*(\mathbf{r}, t) \sum_n E_n(\mathbf{r}, t) \right\rangle \\
&= \left\langle \sum_m |E_m(\mathbf{r}, t)|^2 \right\rangle + \left\langle \sum_{m \neq n} E_m^*(\mathbf{r}, t)E_n(\mathbf{r}, t) \right\rangle \\
&= \sum_m |E_m(\mathbf{r}, t)|^2 + 0. \tag{4}
\end{aligned}$$

60 When the intensity of thermal light is large enough (or the time window long
61 enough) all random phases may be present in the measurement causing the
62 $m \neq n$ terms to sum to zero, leaving just the $m = n$ terms (for which the
63 initial phase information cancels before the summation). Even when present,
64 the $m \neq n$ terms are simply considered as noise, or fluctuations about the mean
65 intensity,

$$\langle I(\mathbf{r}, t) \rangle = \bar{I}(\mathbf{r}, t) + \Delta I(\mathbf{r}, t). \tag{5}$$

66 Traditional imaging processes and interferometers are a result of the mean inten-
67 sity term, or subfields correlated with themselves. This coincides with Dirac's
68 observation that a photon only interferes with itself [9].

69 2. Two-photon Interference

70 By introducing a second detector, intensity correlation measurements can be
71 made such as those demonstrated by Hanbury Brown and Twiss in their stellar
72 interferometer [10, 11]. Using Glauber's formalism, this is known as second
73 order correlation, $\Gamma^{(2)}(\mathbf{r}_1, t_1; \mathbf{r}_2, t_2)$. Like with intensity, the cancellation of the
74 initial phase terms is required to survive the ensemble average. In this case
75 there are two sets of terms that survive: (1) when $m = n$ and $p = q$, and (2)
76 when $m = q$ and $n = p$.

$$\begin{aligned}
\Gamma^{(2)}(\mathbf{r}_1, t_1; \mathbf{r}_2, t_2) &= \langle I(\mathbf{r}_1, t_1)I(\mathbf{r}_2, t_2) \rangle = \langle E^*(\mathbf{r}_1, t_1)E(\mathbf{r}_1, t_1)E^*(\mathbf{r}_2, t_2)E(\mathbf{r}_2, t_2) \rangle \\
&= \left\langle \sum_m E_m^*(\mathbf{r}_1, t_1) \sum_n E_n(\mathbf{r}_1, t_1) \sum_p E_p^*(\mathbf{r}_2, t_2) \sum_q E_q(\mathbf{r}_2, t_2) \right\rangle \\
&= \sum_m |E_m(\mathbf{r}_1, t_1)|^2 \sum_n |E_n(\mathbf{r}_2, t_2)|^2 + \sum_{m \neq n} E_m^*(\mathbf{r}_1, t_1)E_n(\mathbf{r}_1, t_1)E_n^*(\mathbf{r}_2, t_2)E_m(\mathbf{r}_2, t_2) \\
&= \bar{I}(\mathbf{r}_1, t_1)\bar{I}(\mathbf{r}_2, t_2) + \langle \Delta I(\mathbf{r}_1, t_1)\Delta I(\mathbf{r}_2, t_2) \rangle.
\end{aligned} \tag{6}$$

77 It is evident that the $m = n$ and $p = q$ terms correspond to the mean intensities
78 measured at each respective detector D_1 and D_2 . The remaining $m = q$ and
79 $n = p$ terms are simply the correlation of the intensity fluctuation term for D_1
80 and the intensity fluctuation term for D_2 .

$$\langle \Delta I(\mathbf{r}_1, t_1)\Delta I(\mathbf{r}_2, t_2) \rangle = \sum_{m \neq n} E_m^*(\mathbf{r}_1, t_1)E_n(\mathbf{r}_1, t_1)E_n^*(\mathbf{r}_2, t_2)E_m(\mathbf{r}_2, t_2). \tag{7}$$

81 Earlier we stated that the fluctuation term either averages to zero or contributes
82 unwanted noise to the measurement of intensity; however, here we see that this
83 is not the case for intensity fluctuation correlation. The phase information
84 cancels in this measurement, allowing it to survive the ensemble average. Ex-
85 perimentally this can be obtained by measuring the intensity in a series of short
86 time windows at two separate detectors. After obtaining the mean intensity,
87 the fluctuation at each of the time windows can be determined. Then these
88 individual fluctuation terms are correlated with the corresponding terms of the
89 other detector. Averaging these correlated terms gives the final value.

This measurement can be explained as a result of two-photon interference [3]. Comparable to single-photon interference which is apparent through the measurement of intensity (Eq. 4), two-photon interference is a result of a pair of photons interfering with the pair itself. To better visualize this, we can rewrite

equation 6 as the following superposition [3],

$$\langle I(\mathbf{r}_1, t_1)I(\mathbf{r}_2, t_2) \rangle = \sum_{m \neq n} \frac{1}{2} |E_m g_m(\mathbf{r}_1, t_1) E_n g_n(\mathbf{r}_2, t_2) + E_m g_m(\mathbf{r}_2, t_2) E_n g_n(\mathbf{r}_1, t_1)|^2$$

90 Here we clearly see it describes two probability amplitudes for joint detection:
 91 (1) the m th subfield is detected at detector 1 while the n th subfield is detected at
 92 detector 2, *or* (2) the n th subfield is detected at detector 1 while the m th subfield
 93 is detected at detector 2. The cross terms of this superposition are equivalent to
 94 the intensity fluctuation correlation and, in the quantum description, represent
 95 the two probability amplitudes interfering with one another.

96 To better understand the phenomena of two-photon interference, it may be
 97 useful to review the turbulence-free two-photon double-slit interferometer that
 98 has been recently developed [12]. Although not required, a coherent source
 99 like a laser is typically used for a classic double-slit interferometer. It becomes
 100 more difficult to produce an interference pattern in the measurement of intensity
 101 with thermal light due to the spatial coherence of the source: if the source is
 102 too large and the slit separation is greater than the spatial coherence length
 103 ($d \gg l_c$), the light will be incoherent and not produce an interference pattern
 104 [7, 13]. However, two-photon interference through the measurement of intensity
 105 fluctuation correlation is able to produce a fully visible interference pattern even
 106 with fully incoherent light, $d \gg l_c$.

107 When using an incoherent, thermal light source, there are multiple two-
 108 photon amplitudes contributing to the measurement of intensity fluctuation
 109 correlation. Two alternatives that produce an interference pattern are when
 110 the m th subfield propagates from slit-A to detector 1 while the n th subfield
 111 propagates from slit-B to detector 2, *or* the m th subfield propagates from slit-
 112 A to detector 2 while the n th subfield propagates from slit-B to detector 1.
 113 These two-photon probability amplitudes are depicted in figure 1 in blue and
 114 red, respectively. This superposition results in,

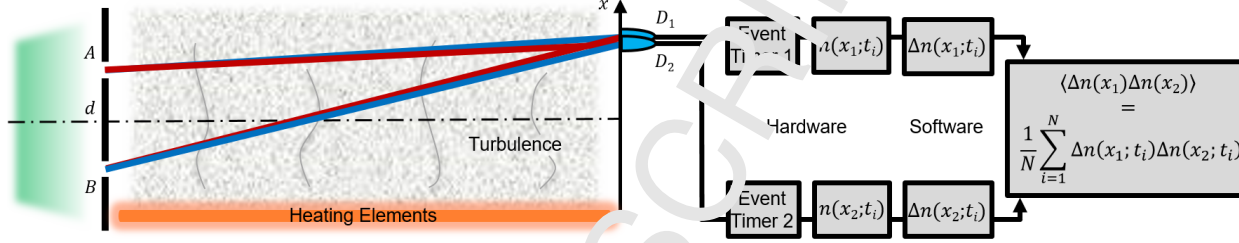


Figure 1: The observed interference is a two-photon phenomenon—a random pair of photons interfering with the pair itself. In the figure, the superposed two different, yet indistinguishable two-photon amplitudes are indicated by red and blue colors. When the detectors are scanning in the neighborhood of $x_1 \approx x_2$, the red amplitude and the blue amplitude “overlap.” This overlap means the pair experience the same phase variations in the red-path and the blue-path. Therefore, the interference will be unaffected by the turbulence.

$$\begin{aligned} \langle \Delta I_{AB}(x_1) \Delta I_{AB}(x_2) \rangle &= \sum_{m \neq n} |E_m|^2 |E_n|^2 g_{mA}^*(x_1) g_{nB}(x_1) g_{mA}(x_2) g_{nB}^*(x_2) \\ &\propto \cos \frac{2\pi d}{\lambda z} (x_1 - x_2). \end{aligned} \quad (8)$$

115 In addition to the above alternatives for the m th and the n th subfields to pro-
 116 duce a joint photodetection event of D_1 and D_2 , the m th and the n th subfields
 117 can also produce a joint photodetection even when both pass through slit-A
 118 or both pass through slit-B. These two alternatives contribute constants to
 119 $\langle \Delta I(x_1) \Delta I(x_2) \rangle$. Adding the contributions from all alternatives, we have an
 120 observable

$$\langle \Delta I(x_1) \Delta I(x_2) \rangle \propto \left[1 + \cos \frac{2\pi d}{\lambda z} (x_1 - x_2) \right]. \quad (9)$$

121 In general, this measurement may be sensitive to turbulence because the random
 122 phase shifts present due to random fluctuations in index of refraction may be
 123 different for each path. Mathematically we can represent the turbulence as a
 124 random phase shift dependent on the path traveled by the subfield. Introducing
 125 this to equation 8 we get,

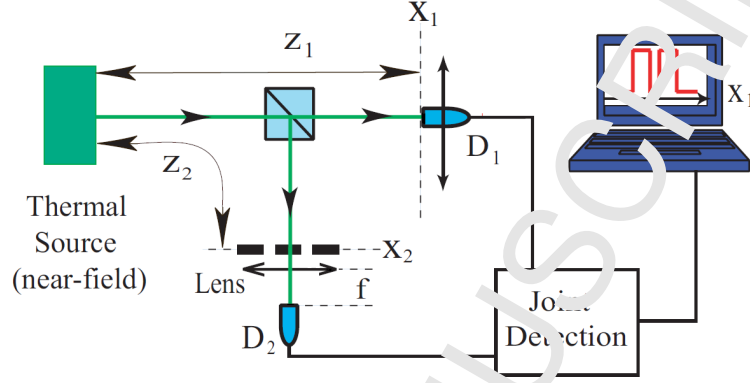


Figure 2: The setup for thermal light ghost imaging consists of a thermal source of radiation, a beam splitter, a scanning point-like detector or detector array, and a bucket detector (shown here as a lens collecting the light to a single detector). The bucket detector collects all of the light from the object as a single measurement, while the detector array does not have a view of object at all.

$$\langle \Delta I_{AB}(x_1) \Delta I_{AB}(x_2) \rangle = \sum_{m \neq n} |E_m|^2 |E_n|^2 g_{mA}^*(x_1) e^{i\delta\phi_A(x_1)} g_{nB}(x_1) e^{-i\delta\phi_B(x_1)} \\ + |E_m|^2 |E_n|^2 g_{mA}^*(x_2) e^{i\delta\phi_A(x_2)} g_{nB}(x_2) e^{-i\delta\phi_B(x_2)} \\ + |E_m|^2 |E_n|^2 g_{mA}^*(x_1) e^{i\delta\phi_A(x_1)} g_{nB}(x_2) e^{-i\delta\phi_B(x_2)} \\ + |E_m|^2 |E_n|^2 g_{mA}^*(x_2) e^{i\delta\phi_A(x_2)} g_{nB}(x_1) e^{-i\delta\phi_B(x_1)}$$
(10)

126 However, a closer look reveals that there is the possibility for cancellation. By
 127 scanning D_1 in a proximately the same location as D_2 ($x_1 \approx x_2$), it is clear
 128 that the pair of two-photon amplitudes, red and blue, overlap (Fig. 1) [12].
 129 Even though each path involves turbulence, the pair of potential paths for the
 130 two-photon experience it by the same magnitude. The resulting interference
 131 pattern is unaffected and maintains full visibility.

132 3. Thermal Light Ghost Imaging

133 Thermal light ghost imaging, shown in Fig. 2, also utilizes a pair of detec-
 134 tors and the measurement of intensity fluctuation correlation [2]. Here a beam
 135 splitter splits light from a thermal source into two paths. One path contains

136 the object of interest (in this case an arbitrary aperture) followed by a bucket
 137 detector which ideally collects all of the light from the object. There is no “res-
 138 olution” needed for this detector so this measurement can be done with a lens
 139 focusing all of the light into a single detector or an array of detectors (such as
 140 a CCD or CMOS array) for which the measurement from each location is later
 141 summed to a single value. The other path from the beam splitter *does* require
 142 spatial information, so a full detector array is used. We will define the array of
 143 detectors as D_1 and the bucket detector as D_2 . For the image to be in focus, the
 144 detector array is placed the same distance from the source (or beam splitter)
 145 as the object, $z_1 = z_2 \equiv d$. Applying this constraint, the intensity fluctuation
 146 correlation produces a sombrero function [7],

$$\langle \Delta I(\boldsymbol{\rho}_1) \Delta I(\boldsymbol{\rho}_2) \rangle \propto \int d\boldsymbol{\rho}_o |A(\boldsymbol{\rho}_o)|^2 \text{somb}^2 \left[\frac{R_s \omega}{d} \left| \boldsymbol{\rho}_1 - \boldsymbol{\rho}_o \right| \right], \quad (11)$$

147 where R_s is the radius of the source and the sombrero (somb) function is defined
 148 as $\text{somb}(x) = 2J_1(x)/x$ where $J_1(\cdot)$ is the first-order Bessel function. The somb
 149 function is the image forming function, transferring a single point on the object
 150 to a “spot” on the image plane. For a source with a large angular diameter,
 151 $\Delta\theta_s = R_s/d$, the point-to-spot somb function can be approximated as a point-
 152 to-point delta function,

$$\langle \Delta I(\boldsymbol{\rho}_1) \Delta I(\boldsymbol{\rho}_2) \rangle \propto \int d\boldsymbol{\rho}_o |A(\boldsymbol{\rho}_o)|^2 \delta(\boldsymbol{\rho}_1 - \boldsymbol{\rho}_o) = |A(\boldsymbol{\rho}_1)|^2. \quad (12)$$

153 Similar to the turbulence-free double-slit interference pattern, if D_1 and D_2
 154 are arranged in such away to achieve path overlap, the measurement of ghost
 155 imaging with thermal light will be insensitive to turbulence. This turbulence-
 156 free mechanism can be extended to ghost imaging by comparing the interfer-
 157 ometer, which has the detectors on the Fourier transform plane, with ghost
 158 imaging, which has the detectors on the imaging plane. On the imaging plane,

159 the path overlap can still be achieved, allowing for measurements insensitive
 160 to turbulence. In 2011, Meyers *et al.* achieved this condition and demon-
 161 strated turbulence-free ghost imaging [14]. It should be noted that other types
 162 of ghost imaging that have been developed do not have this same property.
 163 So far turbulence-free ghost imaging has only been achieved with ghost imag-
 164 ing from intensity fluctuation correlation as a result of two-photon interference.
 165 Other types of ghost imaging such as speckle-speckle correlation, computational
 166 ghost imaging, and ghost imaging with entangled photons are results of different
 167 phenomena, preventing them from being turbulence-free.

168 4. X-ray Ghost Imaging

169 Traditional imaging is dependent on a lens, so will be limited to a certain
 170 range of wavelengths. However, we have seen that ghost imaging does not
 171 require a lens, so photons with higher energy levels such as X-rays can be used.
 172 This leads to a substantial increase in image resolution and allows the imaging
 173 of more objects due to the higher penetrating power of X-rays. Following the
 174 Rayleigh criterion [7, 15], we find that the minimum spatial separation between
 175 resolvable points on the object with ghost imaging is,

$$\Delta x_{GI} \approx \frac{\lambda}{\Delta \theta_s}, \quad (13)$$

176 where $\Delta \theta_s$ is the angular diameter of the source. As an example of how powerful
 177 the use of X-ray can be, let us consider hard X-rays with a wavelength of 0.05
 178 nm ($E \sim 25$ keV) and a source with a angular diameter of approximately 0.05
 179 milliradians, which is achievable for many modern X-ray synchrotron sources
 180 such as the Advanced Photon Source (APS) at Argonne National Laboratory
 181 (FNU). This gives a minimum angular resolution on the order of micrometers,
 182 $\Delta x_{GI} \approx 1 \times 10^{-6}$ m. This is roughly 10,000 times greater image resolution
 183 than using visible light (~ 500 nm) with a comparable angular diameter for

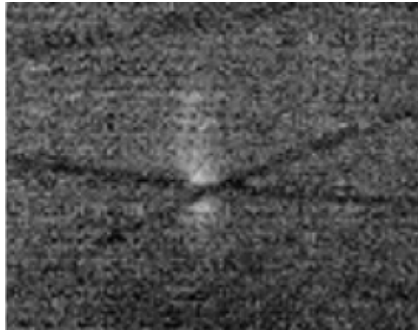


Figure 3: Preliminary tests used the Advanced Photon Source (APS) at Argonne National Laboratory (ANL) to test spatial resolution capabilities of a LYSO scintillator. Here a traditional image was captured of a 20 micrometer wire. Theoretically, the spatial resolution of a LYSO scintillator may be as low as an angstrom.

184 the source. This improvement can be increased even further with higher en-
 185 ergy photons or a larger source, which may be more easily achieved with the
 186 implementation of an X-ray tube as a source, but other limitations may arise.

187 The shift from visible ghost imaging to X-ray ghost imaging may not be
 188 trivial. One of the main obstacles is the beam splitter, which is typically trivial
 189 for visible light. Currently Bragg or Laue diffraction is used, treating one of
 190 the diffracted paths as one path and the transmitted X rays as the other [13].
 191 While functional, this technique is not completely ideal for two reasons: (1)
 192 Due to loss of intensity via absorption and other diffraction paths, the efficiency
 193 of the imaging process is lowered and (2) the split is often not 50/50 which
 194 also reduces the image efficiency. Despite these restrictions, diffraction is
 195 still the most practical option because of cost and proven functionality. Of
 196 interest is the recent development of a kinoform x-ray beam splitter which may
 197 prove to be an option for X-ray ghost imaging in the future [15]. Another
 198 issue is measuring the intensity fluctuations (via intensity measurements) of
 199 the X rays. To accomplish this, it is common to use scintillators to convert
 200 the X rays to visible light which can be measured with visible light detectors
 201 while certain detector arrays have also been developed with the capability to
 202 detect X rays directly. Due to the high resolution of the ghost imaging process,
 203 limiting factors for the images will be dependent on the hardware; such as the
 204 pixel size for the detector array and potentially the spatial resolution of the
 205 scintillator. With recent beam time at the APS we were able to test the spatial
 206 resolution of lutetium yttrium oxyorthosilicate (LYSO:Ce) scintillators and can

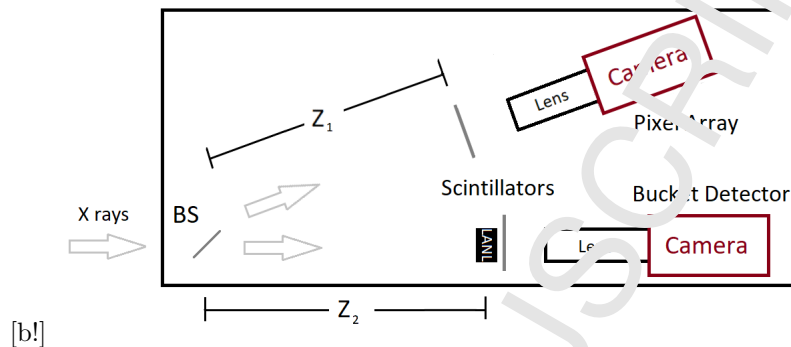


Figure 4: One setup for X-ray ghost imaging consists of a thermal source of X-ray radiation, a “beam splitter” utilizing Laue diffraction, scintillators, and a pair of cameras. The object, represented here as “LANL,” is in the path of the bucket detector and is not seen by the pixel array. The scintillators act as our detection planes and each camera is focused on the corresponding scintillator.

207 confirm that they are acceptable for ghost imaging at the micrometer level
 208 (Fig. 3), and may be able to resolve to the nanometer or angstrom level. LYSO
 209 scintillators (as well as many other scintillators) also had decay times shorter
 210 than the pulse separation at the APS. This temporal resolution of the scintillator
 211 is important to allow for detection of a single pulse, which is preferred for ghost
 212 imaging. Further tests are planned which intend to provide understanding of
 213 how a scintillator affects the measurement of intensity fluctuations.

214 In addition to converting X rays to visible photons, scintillators may have a
 215 use in permitting magnification in our X-ray ghost imaging setup. Unlike tradi-
 216 tional imaging, lensless ghost imaging does not typically result in a magnification
 217 factor. To introduce magnification to optical ghost imaging, it is common to
 218 use a lens to classically image, and magnify, the ghost image plane [2, 14]. This
 219 would be useful for X-ray ghost imaging because magnification would allow for
 220 higher resolution images to be captured by a single detector array. However, as
 221 discussed, the purpose of X-ray ghost imaging was the ability to achieve true
 222 point-to-point imaging with X rays, which are unaffected by a lens. To achieve
 223 these goals, our plan is to further improve the setup as shown in Fig. 4.

224 There has been a growing interest in using synchrotrons and other X-ray
 225 sources for ghost imaging with results reported by multiple groups [16–22]; how-

226 ever, it appears that these techniques are a result of a classical speckle-to-speckle
 227 correlation which does not have the same resolution or turbulence-free capabil-
 228 ities of two-photon interference. Demonstration of true point-to-point imaging
 229 from two-photon interference as well as the turbulence-free and other noise im-
 230 munities of this measurement would be an important step to realize X-ray ghost
 231 imaging in a variety of applications.

232 5. Acknowledgments

233 This work is supported by the C2 program, managed by Dr. Dana Dattel-
 234 baum at Los Alamos National Laboratory.

235 References

- 236 [1] T.B. Pittman, Y.H. Shih, D.V. Stekalov, A.V. Sergienko, Optical imaging
 237 by means of two-photon quantum entanglement, *Phys. Rev. A* **52** (1995)
 238 R3429.
- 239 [2] A. Valencia, G. Scarcelli, M. D’Angelo, Y.H. Shih, Two-photon imaging
 240 with thermal light, *Phys. Rev. Lett.* **94** (2005) 063601.
- 241 [3] G. Scarcelli, V. Berardi, Y.H. Shih, Can two-photon correlation of chaotic
 242 light be considered as correlation of intensity fluctuations? *Phys. Rev. Lett.*
 243 **96** (2006) 063602.
- 244 [4] A. Einstein, Zur elektrodynamik bewegter körper, *Annalen der Physik* **322**
 245 (1905) 891.
- 246 [5] R.J. Glauber, “Photon correlations,” *Phys. Rev. Lett.* **10** (1963) 84.
- 247 [6] R.J. Glauber, The quantum theory of optical coherence, *Phys. Rev.* **130**
 248 (1963) 2529.
- 249 [7] Y. H. Shih, *An Introduction to Quantum Optics: Photon and Biphoton*
 250 *Physics*, 1st ed., CRC press, Taylor & Francis, London, 2011.

- 251 [8] M. O. Scully, M. S. Zubairy, Quantum Optics, Cambridge University Press,
252 Cambridge, England, 1997.
- 253 [9] P. Dirac, The Principle of Quantum Mechanics, Oxford University Press,
254 1930.
- 255 [10] R. Hanbury Brown, R.Q. Twiss, Correlation between photons in two co-
256 herent beams of light, Nature **177** (1956) 27.
- 257 [11] R. Hanbury Brown, R.Q. Twiss, A test of a new type of stellar interferom-
258 eter on Sirius, Nature **178** (1956) 1046.
- 259 [12] T.A. Smith, Y.H. Shih, The turbulence-free double-slit interferometer,
260 Phys. Rev. Lett. **120** (2018) 063606.
- 261 [13] E. Hecht, Optics, Addison Wesley, Reading, MA, 2002.
- 262 [14] R.E. Meyers, K.S. Deacon, F.H. Sun, Turbulence-free ghost imaging, Appl.
263 Phys. Lett. **98** (2011) 111115.
- 264 [15] M. Lebugle, G. Senicinas, F. Marschall, V. A. Guzenko, D. Grolimund, C.
265 David, Tunable blunifform x-ray beam splitter, Opt. Lett. **42**, (2017) 4327.
- 266 [16] H. Yu, R. Lu, S. Han, M. Xie, G. Du, T. Xiao, D. Zhu, Fourier-transform
267 ghost imaging with hard x rays, Phys. Rev. Lett. **117** (2016) 113901.
- 268 [17] D. Pelliccia, A. Rack, M. Scheel, V. Cantelli, D.M. Paganin, Experimental
269 x-ray ghost imaging, Phys. Rev. Lett. **117** (2016) 219902.
- 270 [18] A. Sciarri, S. Shwartz, X-ray ghost imaging with a laboratory source, Opt.
271 Express. **25**, (2017) 14822.
- 272 [19] A.X. Zhang, Y.H. He, L.A. Wu, L.M. Chen, B.B. Wang, Tabletop x-ray
273 ghost imaging with ultra-low radiation, Optica **5**(4) (2018) 374.
- 274 [20] D. Pelliccia, M.P. Olbinado, A. Rack, A.M. Kingston, G.R. Myers, D.M
275 Paganin, Towards a practical implementation of x-ray ghost imaging with
276 synchrotron light, IUCrJ **5** (Pt 4) (2018) 428.

- 277 [21] D. Ceddia, D.M. Paganin, Random-matrix bases, ghost imaging, and x-
278 ray phase contrast computational ghost imaging, *Phys. Rev. A*, **97** (2018)
279 062119.
- 280 [22] A. M. Kingston, D. Pelliccia, A. Rack, M. P. Ollinado, J. Cheng, G. R.
281 Myers, D. M. Paganin, Ghost tomography, *Optica* **5**, (2018) 1516.